

# Investigation of Coherent Diffraction Radiation from a Dual Target system at CTF3 and its application for longitudinal bunch profile diagnostics

Konstantin Lekomtsev,\* Grahame Blair, Gary Boorman, and Pavel Karataev  
*John Adams Institute at Royal Holloway University of London, Egham, Surrey, TW20 0EX, UK.*

Roberto Corsini and Thibaut Lefevre  
*CERN CH-1211, Geneva 23, Switzerland.*

(Dated: October 28, 2011)

A Coherent Diffraction Radiation (CDR) experiment was built at the CLIC Test Facility 3 at CERN. Two silicon wafers are positioned on one side of the beam and a CDR radiation, originated from them, is translated towards a Michelson Interferometer. The first target cuts off the backgrounds, generated by the beam from upstream of the experimental setup. Online bunch length monitoring, based on detection of a coherent radiation spectrum, is a promising technique, providing the single electron spectrum is predictable. However, an idealised theory along with coherent backgrounds, generated by the beam, complicate the result interpretation. In this paper the results of the theoretical and experimental investigations of the CDR from the two targets and a work towards longitudinal diagnostics of sub-picosecond electron bunches is presented. A theoretical model, which describes a spatial distribution of the CDR, was developed for the new dual target configuration. The radiation spatial distribution measurements were performed and compared with the theory. A capability to obtain interferometric measurements of CDR at the experimental setup was proven. Bunch shape instabilities at CTF3 were investigated, as well.

**PACS 41.60.-m:** Radiation by moving charges.

**PACS 41.75.-i:** Charged-particle beams.

## I. INTRODUCTION

Diffraction Radiation (DR) is a physical phenomenon occurring when a charged particle moves in the vicinity of a conducting screen. The coulomb field of the particle interacts with the screen and surface currents are produced, which become a source of the DR. A theory of DR was developed in 1950s, however, the first experimental investigations were performed only in 1995 by Shibata et al. [1]. Using an electron beam with the energy of 150 MeV, the DR was generated by a circular aperture in millimetre and submillimetre wavelength regions.

The DR generated from conducting screens has been experimentally investigated in the last 15 years [2–4] and it was proven to be very promising tool for the longitudinal [5, 6] and transverse [7, 8] diagnostics of electron beams. The main advantage of DR compared to Transition Radiation, for instance, that it doesn't affect the beam. Other important property of this physical phenomenon is instantaneous emission, which makes it possible to perform single shot, time resolved measurements. Experiment-wise one is interested in observation of the, so called, Coherent Diffraction Radiation (CDR), due to the fact that coherent radiation is  $N$  times more intensive than incoherent radiation, where  $N$  is the number of particles in the beam. The coherency of the effect is achieved when the electrons in a bunch radiate in phase, i.e. a wavelength of radiation is comparable or larger than the bunch length.

A novel scheme for the drive beam generation has been proposed for the future Compact Linear Collider (CLIC), in which a long bunch train with a low bunch repetition frequency will be accelerated with a low RF frequency and, then, recombined to increase the bunch repetition frequency by more than an order of magnitude. The optimisation and monitoring of the longitudinal charge distribution in the bunch is crucial for an optimal performance of the CLIC drive beam as well as for maximization of the luminosity at the CLIC interaction point [9].

At the CLIC Test Facility 3 we have built an experimental setup based on the CDR from a Dual Target system. Two silicon wafers, coated with aluminium, are positioned on one side of the beam and the radiation, generated from them, is translated towards a Michelson Interferometer. The upstream target serves as a barrier for the Coherent Synchrotron Radiation (CSR) backgrounds coming from upstream of the experimental setup, Figure 1. The ultimate goal of the experiment is to reconstruct a bunch shape from the spectral measurements, obtained at the Michelson interferometer. In the current configuration of the setup narrow-band Schottky Barrier Diode (SBD) detectors are used for the spectral measurements. The intensity of CDR is defined by the following equation:

$$S(\omega) = S_e(\omega)N^2F(\omega), \quad (1)$$

where  $S(\omega)$  is the measured spectrum,  $S_e(\omega)$  is the single electron spectrum and it has to be predicted precisely,  $N$  is the number of electrons in the bunch;  $F(\omega)$  is the bunch form factor which contains information about the longitudinal distribution of electrons in the bunch.

---

\* Konstantin.Lekomtsev.2009@live.rhul.ac.uk

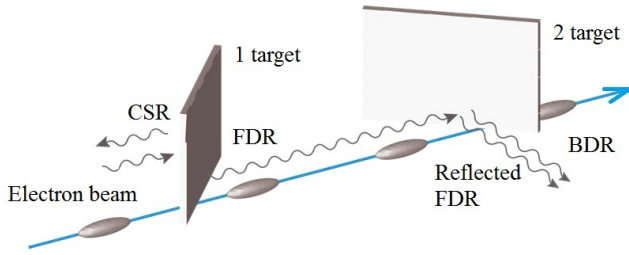


FIG. 1. Schematic layout of the Dual Target System at CTF3. FDR - Forward Diffraction Radiation; BDR - Backward Diffraction Radiation; CSR - Coherent Synchrotron Radiation.

In this paper the Coherent Diffraction Radiation experiment will be discussed in great detail. Theoretical investigations as well as experimental measurements of the CDR spatial distributions will be shown. Interferometric measurement of the CDR from the dual target system will be reported. Bunch shape and length instabilities at CTF3 will be discussed, as well.

## II. CALCULATION OF CDR FROM THE TARGETS

### A. Backward Diffraction Radiation from the second target

For the calculations we shall use a classical theory of Diffraction Radiation, based on Huygens principle of plane wave diffraction. In reality, the classical theory describes backward DR only. However, for a metallic foil and millimetre wavelengths we can use an ideal conductor approximation. In this case backward DR characteristics coincide with forward DR ones [10]. A particle field is introduced as a superposition of its pseudo-photons and when they are scattered off a target surface, they are converted into the real ones and propagate either in the direction of the specular reflection (BDR) or along the particle trajectory (FDR).

In this subsection we consider the radiation from the

second target only, excluding influence of the first target at all. Consider an electron moving along the  $z$ -axis. Each point of a target surface can be represented as an elementary source of the radiation. Two polarisation components of the DR can be represented as a superposition of the waves from all elementary sources at a distance  $\mathbf{r}$  from the target:

$$E_r = -\frac{1}{4\pi^2} \iint E'(x_r, y_r) \frac{e^{ik|\mathbf{r}|}}{r} dx_r dy_r. \quad (2)$$

$E'(x_r, y_r)$  is the amplitude of the radiation source positioned on the target surface,  $(x_r, y_r)$  are the coordinates of the radiation source on the target surface,  $r$  is the distance from the radiation source at the target to the observation point.

The amplitude  $E'(x_r, y_r)$  can be represented as a Fourier transform of the incident particle field [10]:

$$\begin{aligned} E'(x_r, y_r) &= -\frac{ie}{2\pi^2} \iint \frac{k'_{x,y} \exp[i(k'_x x_r + k'_y y_r)]}{k_x'^2 + k_y'^2 + k^2 \gamma^{-2}} dk'_x dk'_y \\ &= \frac{ek}{\pi\gamma} \frac{x_r, y_r}{\sqrt{x_r^2 + y_r^2}} K_1 \left( \frac{k}{\gamma} \sqrt{x_r^2 + y_r^2} \right), \end{aligned} \quad (3)$$

where  $k$  is the wave number,  $\lambda$  is the wavelength of the DR,  $\gamma$  is the Lorentz-factor,  $k'_{x,y}$  are the components of the electron pseudo-photon wave vector,  $K_1$  is a modified Bessel function of the first order.

Parameters  $(\xi - x_r)/a$  and  $(\eta - y_r)/a$ , where  $\xi$  and  $\eta$  are the coordinates at the observation plane, determine the angles of the photon emission by an elementary radiation source and in ultra-relativistic case they are of order of  $\gamma^{-1}$ . Therefore, a phase term of the photons propagating from the target to the observation plane can be written as follows [11]:

$$\begin{aligned} \frac{\exp(ik|\mathbf{r}|)}{|\mathbf{r}|} &\approx \frac{\exp(ika)}{a} \exp \left[ \frac{ik}{2a} (x_r^2 + y_r^2) - \frac{ik}{a} (x_r \xi + y_r \eta) \right. \\ &\quad \left. + \frac{ik}{2a} (\xi^2 + \eta^2) \right]. \end{aligned} \quad (4)$$

Consequently two polarisation components of the DR from the second target can be written as [12]:

$$E_{r_2}^2(\xi, \eta) = -\frac{1}{4\pi^2} \frac{ek \exp(ika)}{\pi\gamma a} \iint \left( \frac{x_2}{\sqrt{x_2^2 + y_2^2}} \right) K_1 \left( \frac{k}{\gamma} \sqrt{x_2^2 + y_2^2} \right) \exp \left[ \frac{ik}{2a} ((x_2 - \xi)^2 + (y_2 - \eta)^2) \right] dx_2 dy_2, \quad (5)$$

where  $x_2$  and  $y_2$  are the coordinates at the target surface and  $a$  is the distance between the target and the observation plane.

The DR spatial distribution in a general form can be written as:

$$\frac{d^2 W^{DR}}{d\omega d\Omega} = 4\pi^2 k^2 a^2 (|E_x^{DR}|^2 + |E_y^{DR}|^2), \quad (6)$$

where  $E_x^{DR}$  and  $E_y^{DR}$  are the horizontal and vertical polarisation components of the DR, respectively. If one

needs to obtain a spatial distribution of the BDR from the second target Eq. 5 has to be substituted into Eq. 6.

### B. Forward Diffraction Radiation from the first target

Assuming that for our wavelength and a metallic foil FDR and BDR are identical we can calculate the FDR

---


$$E_{r_1}^{1 \rightarrow 2}(x_2, y_2) = -\frac{1}{4\pi^2} \frac{ek \exp(ikd)}{\pi\gamma d} \iint \left( \frac{x_1}{\sqrt{x_1^2 + y_1^2}} \right) K_1 \left( \frac{k}{\gamma} \sqrt{x_1^2 + y_1^2} \right) \exp \left[ \frac{ik}{2d} ((x_1 - x_2)^2 + (y_1 - y_2)^2) \right] dx_1 dy_1, \quad (7)$$

where  $x_1, y_1$  are the coordinates at the first target surface and  $d$  is the distance between the targets.

Reflection of the FDR at the second target surface and further propagation of the radiation towards the observation plane can be calculated simply by multiplication of Eq. 7 by the phase term of the photons, propagating from the second target to the observation plane. The

from the first target at the observation plane, which is rather complex process, because we have to take into account propagation of the radiation towards the second target and, then, diffraction from it. The first stage of the process, electric field of the FDR produced at the first target and propagating towards the second one, can be written as:

phase term can be written as:

$$\frac{\exp(ika)}{a} \exp \left[ \frac{ik}{2a} (x_2^2 + y_2^2) - \frac{ik}{a} (x_2\xi + y_2\eta) + \frac{ik}{2a} (\xi^2 + \eta^2) \right], \quad (8)$$

The spatial distribution of the FDR diffracted from the second target is the following:

---


$$E_{r_1}^1(\xi, \eta) = -\frac{1}{4\pi^2} \frac{ek \exp(ik(d+a))}{\pi\gamma ad} \frac{k}{2\pi i} \iiint \left( \frac{x_1}{\sqrt{x_1^2 + y_1^2}} \right) K_1 \left( \frac{k}{\gamma} \sqrt{x_1^2 + y_1^2} \right) \times \exp \left[ \frac{ik}{2d} ((x_1 - x_2)^2 + (y_1 - y_2)^2) + \frac{ik}{2a} ((x_2 - \xi)^2 + (y_2 - \eta)^2) \right] dx_1 dy_1 dx_2 dy_2. \quad (9)$$

For the further calculations we rearrange the terms and replace the integration over  $x_2$  and  $y_2$  with the combination of Fresnel's integrals. This allows us to use a rational approximation of the Fresnel's integrals in order

to reduce the calculation time and increase performance of the code (see Appendix A). Therefore, we can obtain the final result for Eq. 9 [12]:

---


$$E_{r_1}^1(\xi, \eta) = \frac{ie \exp[ik(a+d)]}{4\pi^2 \lambda \gamma (a+d)} \iint \left( \frac{x_1}{\sqrt{x_1^2 + y_1^2}} \right) K_1 \left( \frac{k}{\gamma} \sqrt{x_1^2 + y_1^2} \right) \times \left( \left[ \cos \left[ \frac{k}{2(a+d)} ((x_1 - \xi)^2 + (y_1 - \eta)^2) \right] (T_1 T_2 - T_3 T_4) - \left[ \sin \left[ \frac{k}{2(a+d)} ((x_1 - \xi)^2 + (y_1 - \eta)^2) \right] (T_1 T_4 + T_3 T_2) \right] + i \left[ \cos \left[ \frac{k}{2(a+d)} ((x_1 - \xi)^2 + (y_1 - \eta)^2) \right] (T_1 T_4 + T_3 T_2) + \left[ \sin \left[ \frac{k}{2(a+d)} ((x_1 - \xi)^2 + (y_1 - \eta)^2) \right] (T_1 T_2 - T_3 T_4) \right] \right) dx_1 dy_1, \quad (10)$$

where  $T_1 = T_1(x_1, \xi), T_2 = T_2(y_1, \eta), T_3 = T_3(x_1, \xi), T_4 = T_4(y_1, \eta)$  (see Appendix B) are the terms

containing the Fresnel's integrals.

### C. Diffraction Radiation from the two targets

Once the two radiation components are obtained, the DR distribution from the two targets can be derived. The interference between the BDR from the second target and the FDR from the first target is observed, therefore the following formula for the radiation spatial distribution is applied:

$$\frac{d^2W_r^{DR}}{d\omega d\Omega} = 4\pi^2 k^2 a^2 \left[ \left( \text{Re}E_{r_1}^1 - \text{Re} \left[ E_{r_2}^2 \exp\left(\frac{ikd}{\beta}\right) \right] \right)^2 + \left( \text{Im}E_{r_1}^1 - \text{Im} \left[ E_{r_2}^2 \exp\left(\frac{ikd}{\beta}\right) \right] \right)^2 \right], \quad (11)$$

where  $E_{r_1}^1$  and  $E_{r_2}^2$  are the FDR from the first target and the BDR from the second target, correspondingly, which were calculated in the previous subsections;  $\beta = v/c$  is the speed of an electric charge in terms of the speed of light. The  $\exp(ikd/\beta)$  defines the phase delay due to the particle moving from the first target to the second one.

Understanding of the radiation distribution geometry is crucially important for optimisation of the experimental setup. In the current configuration the two targets are positioned on one side of the beam, therefore the fields of DR interfere with each other. The CDR distributions as functions of the second target impact parameter and the horizontal coordinate at the observation plane were calculated for the two main configurations of the experiment. The first configuration: the impact parameter of the first (upstream) target is much larger than the impact parameter of the second (downstream) target. The second configuration: the targets are positioned at the same distance from the beam.

In Figure 2 and 3 the vertical polarisation component of the CDR spatial distribution is presented for the two main configurations of the setup. The distributions have a single mode nature and for the situation when both targets are at the same distance from the beam, Figure 3, a destructive interference is observed, which manifests itself in 50 percent decrease of the radiation intensity.

The spatial distribution of the horizontal polarisation component of the radiation has a dual mode nature, which can be seen in Figures 4 and 5. It is worth noting, that as opposed to the vertical polarisation the intensities of the CDR from the two targets add up for the second configuration of the targets.

## III. EXPERIMENTAL INVESTIGATION OF CDR FROM A DUAL TARGET SYSTEM.

### A. Experimental setup

The experimental setup is located at the Combiner Ring Measurements (CRM) line of the CLIC Test Facility 3 (CTF3). The CRM line is a straight section deviated

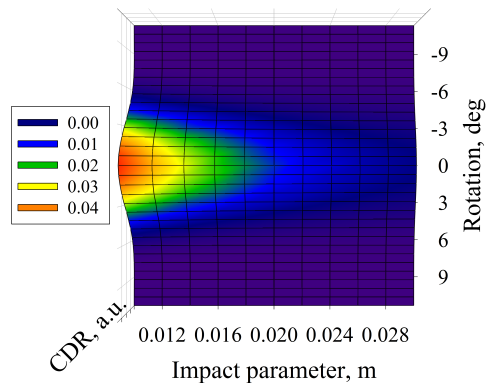


FIG. 2. Vertical polarisation of the CDR distribution. The targets impact parameters  $h_1=30\text{mm}$ ;  $h_2=10\text{mm}$ .

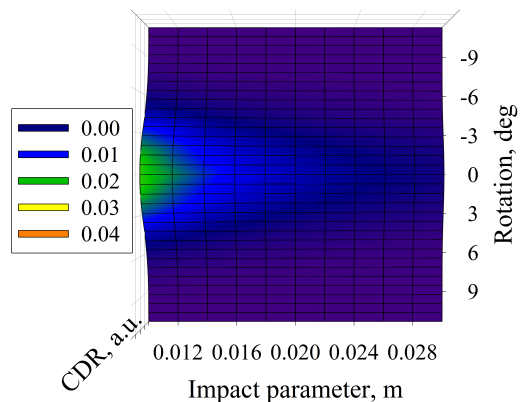


FIG. 3. Vertical polarisation of the CDR distribution. The targets impact parameters  $h_1=10\text{mm}$ ;  $h_2=10\text{mm}$ .

from the first quarter of the Combiner Ring, Figure 6. Once the bending magnet, located at the entrance to the CRM line, is switched off, the beam is directed straight into the beam dump and the CDR from the targets can be observed. If the bending magnet is switched on a Coherent Synchrotron Radiation (CSR), generated upstream of the experimental setup, can be measured.

Two six-way crosses are installed at the CRM line, they contain two targets, which are positioned above the beam at 45deg with respect to the beam propagation direction. The targets are silicon wafers coated with aluminium, they are attached to the Ultra High Vacuum (UHV) manipulators, which provide the vertical translation and rotation of the second target and a vertical translation of the first target.

The radiation, originated from the targets, is transferred through a CVD diamond window with a viewing diameter of 30 mm. Diamond exhibits a broadband transparency in the far-infrared and millimetre wavelength range. The CVD window has a thickness of 0.5 mm, which is smaller than or comparable to the observation wavelength and, therefore, the viewport absorption and the distortion of the transmitted radiation spectrum due to multiple reflections are minimized. The radiation,

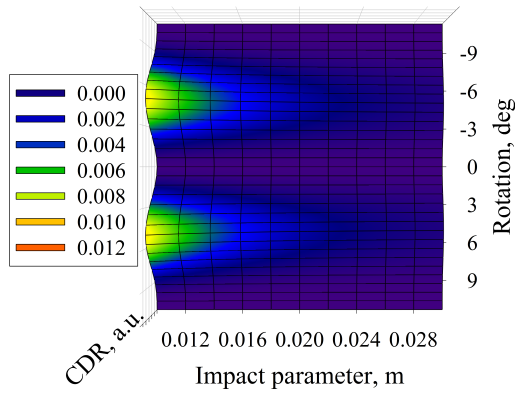


FIG. 4. Horizontal polarisation of the CDR distribution. The targets impact parameters  $h_1=30\text{mm}$ ;  $h_2=10\text{mm}$ .

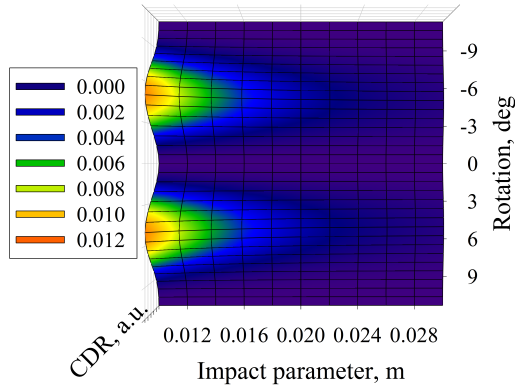


FIG. 5. Horizontal polarisation of the CDR distribution. The targets impact parameters  $h_1=10\text{mm}$ ;  $h_2=10\text{mm}$ .

originated from the targets, is translated vertically by a periscope towards the floor to avoid X-ray backgrounds from the horizontal particle beam plane. On the optical table a Michelson interferometer is installed, Figure 7.

The polariser (P1) transmits the vertical polarisation component towards the interferometer and reflects the horizontal polarisation component toward the second detector, positioned beside the interferometer and used for bunch shape instability studies. The parameters of the experimental setup and CTF3 are presented in Table I.

In the experiment the ultra fast Schottky barrier diode (SBD) detectors with a response time typically around

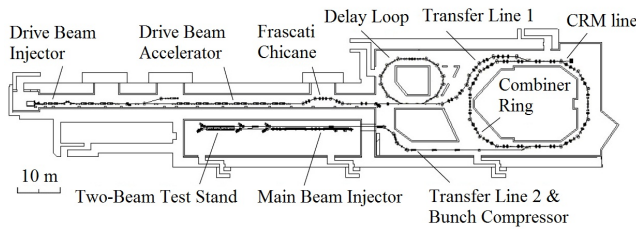


FIG. 6. Schematic layout of the CLIC Test Facility 3.

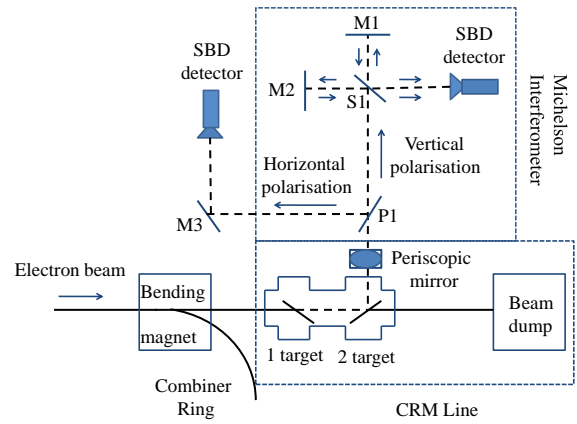


FIG. 7. Schematic layout of the CDR experiment.

TABLE I. CTF3 and CDR experiment parameters.

Parameter	Value	Unit
Beam energy ( $\gamma$ )	235	
Bunch charge	2.3	nC
Bunch spacing frequency	1.5 or 3	GHz
Target dimensions (projected)	40x40	mm
Observation wavelength ( $\lambda$ )	5	mm
First target impact parameter ( $h_1$ ) (upper position)	30	mm
First target impact parameter (lower position)	10	mm
Second target impact parameter ( $h_2$ )	10	mm
Distance between the targets ( $d$ )	0.25	m
Distance from the second target to the observation plane ( $a$ )	2	m

250 ps are used to measure power in the narrow frequency ranges. The detectors are sensitive in 50 - 75 GHz (DXP15), 60 - 90 GHz (DXP12) and 40 - 60 GHz (DXP19). They are polarisation sensitive and only one detector can be used at a time for the interferometric measurements.

Data acquisition is performed using a 10-bit Acqiris DC282 digitiser. The digitiser can provide four channel sampling at up to 2 GS/s, or dual and single-channel sampling at 4 Gs/s and 8 Gs/s, respectively. In the current configuration 4Gs/s sampling for two channels is used. The input for an external trigger provides a precise synchronisation with the electron gun trigger. The data is read out for every single bunch train and transferred to the digitiser through high quality RF cables.

In the following section the results of the CDR spatial distribution measurements for the two main configurations of the experimental setup will be presented.

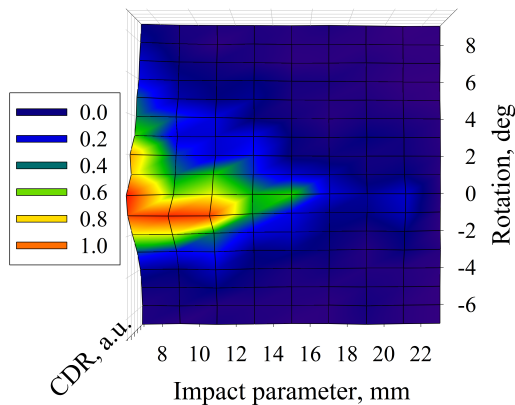


FIG. 8. Vertical polarisation of the CDR distribution measured by DXP15 detector. The targets impact parameters  $h_1=27\text{mm}$ ;  $h_2=7\text{mm}$ .

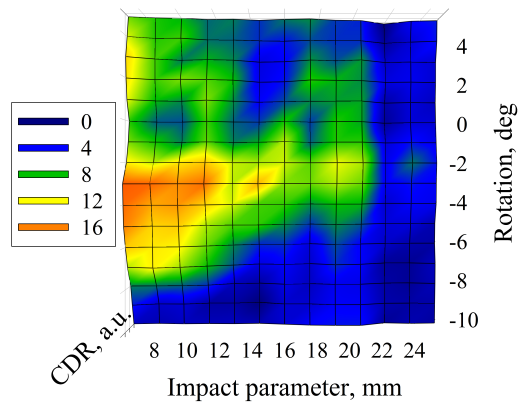


FIG. 10. Horizontal polarisation of the CDR distribution measured by DXP15 detector. The targets impact parameters  $h_1=30\text{mm}$ ;  $h_2=7\text{mm}$ .

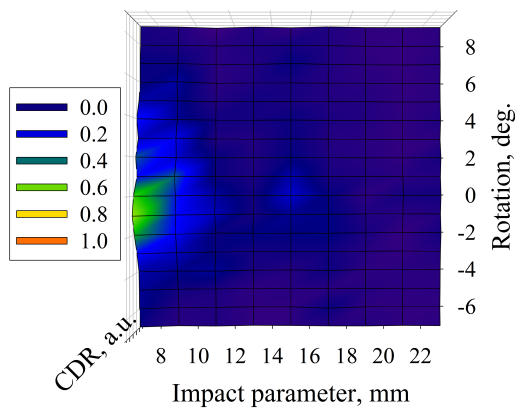


FIG. 9. Vertical polarisation of the CDR distribution measured by DXP15 detector. The targets impact parameters  $h_1=7\text{mm}$ ;  $h_2=7\text{mm}$ .

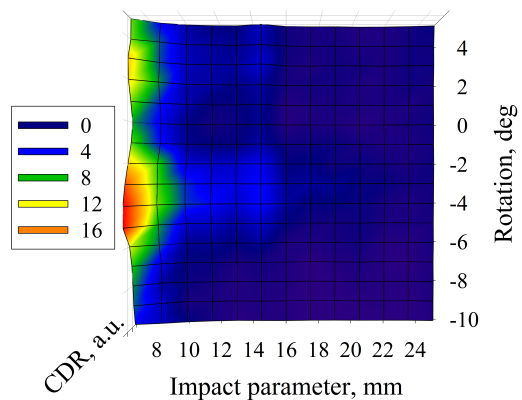


FIG. 11. Horizontal polarisation of the CDR distribution measured by DXP15 detector. The targets impact parameters  $h_1=7\text{mm}$ ;  $h_2=7\text{mm}$ .

## B. Measurements of the CDR spatial distribution

The CDR spatial distributions as functions of the second target's rotation angle and the impact parameter were measured for the two main configurations of the experimental setup. In Figures 8 and 9 the vertical polarisation components of the CDR distributions, measured by the detector sensitive in 50-75 GHz and normalised by the beam current, are presented. In Figure 9 the intensity of the radiation is suppressed due to the destructive interference between the two targets. The distributions have a single mode nature which agrees with the theoretical calculations, Figures 2 and 3. It is worth noting that for the first configuration of the targets, Figure 8, a contribution of the coherent backgrounds coming from upstream of the experimental setup is not suppressed, which leads to a distortion of the spatial distribution.

In Figures 10, 11 the horizontal polarisation components of the CDR spatial distribution, measured using DXP15 detector, are shown. According to the theory, Figures 4 and 5, the horizontal polarisation component

of the CDR from the dual target system has a dual mode nature, moreover, increase in the intensity of radiation is observed for the second configuration of the targets, i.e. when they are positioned at the same distance from the beam. As for the experimental measurements, an inequality of the peaks' intensities can be seen and will require additional studies. In Figure 11 a slight increase of the radiation intensity is, also, observed, which is in agreement with the theoretical model.

In Figures 10 and 11 the ability of the first (upstream) target to block the backgrounds coming from upstream of the experimental setup is demonstrated, as well. The distribution in Figure 10 is significantly more distorted by the coherent backgrounds, than the radiation distribution in Figure 11 where the background contribution is suppressed by the first target [13].

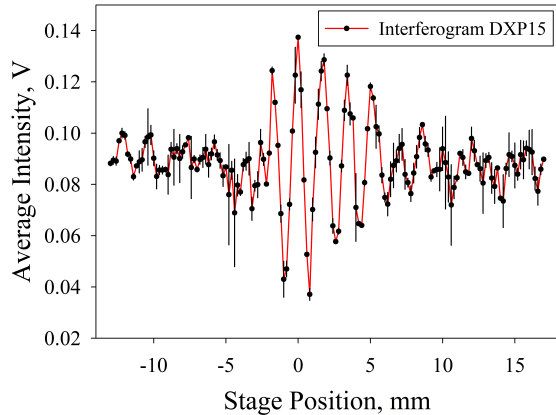


FIG. 12. A sample interferogram obtained for the dual target system.

#### IV. INTERFEROMETRIC MEASUREMENTS

The Michelson interferometer is used to perform spectral measurements of the CDR, originated from the targets. The measurements are performed in the following way: a detector in the interferometer registers vertical polarisation component of the radiation; the DAQ system reads out a signal from the detector for each train of bunches; an interferometric scan is performed by moving the mirror M1 (Figure. 7) on the translation stage; three to ten signal readouts per position of the M1 are performed to collect statistics. A length of the interferometric scan can vary and it was limited to the maximum traveling range of the translation stage (100mm for UTS100 stage, which was in use at a time of the measurement).

Each point of the interferogram is obtained by calculating the average integrated intensity of the CDR radiation over the number of signals, obtained per position of the mirror. The integration for each signal is performed over a narrow slice of the pulse (approximately 50 ns), this is done, mainly, to eliminate the contribution of too many frequencies into the interferometric measurement. A sample interferogram, obtained while both targets are at the same distance from the beam, is presented in Figure 12. A sample signal of the detected radiation with the marked integration region is presented in Figure 13.

The measurement was performed using DXP15 detector when both target were at 7mm from the beam; the stage traveling range for the measurement was  $x = 30\text{mm}$  which resulted in the path difference of  $z = 2x = 60\text{mm}$  and the corresponding signal delay in the interferometer of  $T = z/c = 200\text{ps}$ . This yields the maximum spectral resolution of 5GHz. The DXP15 detector is sensitive in 50-75 GHz, which gives five spectral data points in this frequency region. Due to the low number of data points and a very narrow frequency region this measurement has a very limited applicability for a bunch profile

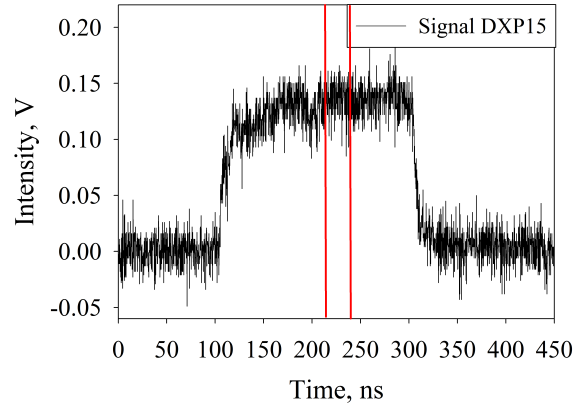


FIG. 13. A sample signal from the DXP15 detector.

reconstruction.

A bunch length stability along the train is a key to successful spectral measurements. When the bunch length vary along the pulse the Coherent Diffraction Radiation is generated at different wavelengths from different parts of the pulse, therefore complicating the result interpretation. Additional problematic issue is instability of a bunch shape. At CTF3 bunch length manipulations are performed before the beam is inserted in to the recombination rings and after it is extracted from them. In the linac section of CTF3 the bunch length is in the region of 1 to 7 ps, then the beam is directed through the stretching chicane where the bunches are stretched up to 15 to 20 ps to achieve effective recombination in the Delay Loop and the Combiner Ring, later on, the bunches are shortened to 1-2 ps to achieve an effective RF transfer in the Power Extraction and Transfer Structures (PETS), Figure 6. When the beam goes through the Frascati chicane the bunches can become distorted and micro-bunching structures can occur, which results in distortion of the signals, obtained using the high frequency SBD detectors.

At CTF3 there is a possibility to provide a real-time monitoring of the bunch length variation along the pulse using the detectors, installed in the interferometric system. There is, also, a RF - pickup hardware, installed in the Transfer Line 1 of CTF3, which consists of a single WR28 waveguide pickup, attached to the beam pipe and separated by a thin vacuum window. The power is detected by an SBD detector, sensitive in 26.5 - 40 GHz [14]. In Figure 14 the signals from the the DXP19 detector sensitive in 40-60 GHz and the waveguide pickup are presented. The shape of the signals most likely signifies significant bunch shape variation along the train, as both of the diagnostics are positioned after the Frascati chicane and the signals from the RF-pickups in the Linac before the chicane generally demonstrate more flat signals. It is, also, worth noting that the signals are very sensitive to the phase variation of the first two klystrons

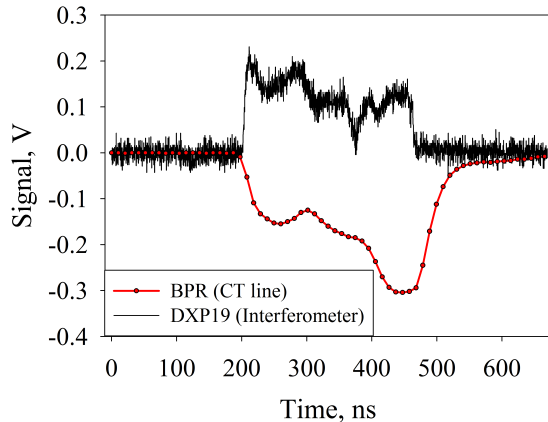


FIG. 14. Signals from the DXP19 detector in the interferometer and the RF-pickup in the Transfer Line 1.

in the Linac which is in addition to the long-term drifts of the latter significantly complicate obtaining of fairly lengthy interferometric scans, which take 7 to 15 minutes to take.

Overall, the experimental setup was proved to be capable of taking interferometric data despite significant bunch shape instabilities and the RF drifts in the machine. As an immediate solution of a bunch shape variation problem could be installation of the low frequency detectors, which would be less sensitive to the changes of a bunch shape.

## V. CONCLUSIONS AND OUTLOOK

In this paper the results of the Coherent Diffraction Radiation experiment were presented. The theoretical model, based on the Classical Diffraction Radiation theory, was developed for the dual target system of the experimental setup. The CDR spatial distributions were calculated for the two main configurations of the targets. The theoretical calculations were in general agreement with the measured spatial distributions. However, certain adjustments to the photon phase terms in the theoretical model should be introduced in order to describe the horizontal polarisation component of the radiation more accurately. The upstream target was proved to be an effective obstacle for the CSR backgrounds coming from upstream of the experimental setup.

The proof of principle measurements showed that interferometric measurements can be performed at the new two target configuration. Bunch length and shape instabilities and their influence on the measurements were discussed. A clear understanding of the problematic issues and the hardware constraints was achieved. The ways towards the further development of the experimental setup were identified: firstly, usage of low frequency detectors in the interferometer to suppress the influence

of bunch shape variations and, secondly, as a more long term-solution, shot-by-shot measurements and installation of a grating spectrometer in the interferometer.

## Appendix A: Fresnel's Integrals

We shall consider two types of the Fresnel's integrals  $C(z) = \int_0^z \cos\left(\frac{\pi}{2}t^2\right) dt$  and  $S(z) = \int_0^z \sin\left(\frac{\pi}{2}t^2\right) dt$  and rational approximation for them [15]:

$$C(z) = \frac{1}{2} + \frac{1 + 0.926z}{2 + 1.792z + 3.104z^2} \sin\left(\frac{\pi}{2}z^2\right) - \frac{1}{2 + 4.142z + 3.492z^2 + 6.67z^3} \cos\left(\frac{\pi}{2}z^2\right), \quad (\text{A1})$$

$$S(z) = \frac{1}{2} - \frac{1 + 0.926z}{2 + 1.792z + 3.104z^2} \cos\left(\frac{\pi}{2}z^2\right) - \frac{1}{2 + 4.142z + 3.492z^2 + 6.67z^3} \sin\left(\frac{\pi}{2}z^2\right). \quad (\text{A2})$$

The considered Fresnel's integrals also follow the rule:

$$C(z) = \begin{cases} C(z) & \text{if } z > 0 \\ -C(|z|) & \text{otherwise;} \end{cases} \quad (\text{A3})$$

$$S(z) = \begin{cases} S(z) & \text{if } z > 0 \\ -S(|z|) & \text{otherwise.} \end{cases} \quad (\text{A4})$$

## Appendix B: $T_i$ terms

The terms  $T_i$  containing the Fresnel's integrals can be expressed as:

$$T_1(x_1, \xi) = C(t_1(x_1, \xi)) - C(t_2(x_1, \xi)), \quad (\text{B1})$$

$$T_2(y_1, \eta) = C(t_3(y_1, \eta)) - C(t_4(y_1, \eta)), \quad (\text{B2})$$

$$T_3(x_1, \xi) = S(t_1(x_1, \xi)) - S(t_2(x_1, \xi)), \quad (\text{B3})$$

$$T_4(y_1, \eta) = S(t_3(y_1, \eta)) - S(t_4(y_1, \eta)), \quad (\text{B4})$$

where

$$t_1(x_1, \xi) = \sqrt{\frac{2(a+d)}{\lambda ad}} \left( x_{\text{height}} + \text{impact} - \frac{ad}{a+d} \left( \frac{x_1}{d} + \frac{\xi}{a} \right) \right), \quad (\text{B5})$$

$$t_2(x_1, \xi) = \sqrt{\frac{2(a+d)}{\lambda ad}} \left( \text{impact} - \frac{ad}{a+d} \left( \frac{x_1}{d} + \frac{\xi}{a} \right) \right), \quad (\text{B6})$$

$$t_3(y_1, \eta) = \sqrt{\frac{2(a+d)}{\lambda ad}} \left( \frac{y_{width}}{2} - \frac{ad}{a+d} \left( \frac{y_1}{d} + \frac{\eta}{a} \right) \right), \quad (\text{B7})$$

$$t_4(y_1, \eta) = \sqrt{\frac{2(a+d)}{\lambda ad}} \left( -\frac{y_{width}}{2} - \frac{ad}{a+d} \left( \frac{y_1}{d} + \frac{\eta}{a} \right) \right), \quad (\text{B8})$$

$x_{height} + impact$  and  $impact$  are the coordinates which

correspond to the upper and the lower edges of the target, and  $-y_{width}/2$  with  $y_{width}/2$  correspond to the left and right edges of the targets.

## ACKNOWLEDGMENTS

Work supported by the EU under contract PITN-GA-2008-215080.

- 
- [1] Shibata Y. et al., *Physical Review E*, **52** 6787 (1995).  
 [2] Vnukov I.E. et al., *JETP Letters*, **67** 802 (1998).  
 [3] Urakawa J. et al., *Nuclear Instruments and Methods, A* **472** 309 (2001).  
 [4] Muto T. et al., *Physical Review Letters*, **90** 104801-1 (2003).  
 [5] Feng B. et al., *Nuclear Instruments and Methods, A* **475** 492 (2001).  
 [6] Castellano M. et al., *Physical Review, E* **63** 056501-1 (2001).  
 [7] Karataev P. et al., *Physical Review Letters*, **93** 244802 (2004).  
 [8] Karataev P. et al., *Nuclear Instruments and Methods, B* **227** 158 (2005).  
 [9] Geschonke G. et al., *CTF3 Design report 2002-08*, CERN/PS (2002).  
 [10] Ter-Mikaelyan M.L., *High Energy Electromagnetic Processes in Condensed Media*, (New York: Wiley-Interscience) (1972).  
 [11] Karataev P. et al., *Phys. Lett. , A* **345** 428 (2005).  
 [12] Lekomtsev K. et al., *IL NUOVO CIMENTO*, **34C** N4 261 (2011).  
 [13] Lekomtsev K. et al, Investigation of Coherent Diffraction Radiation from a Dual Target system at CTF3, *Journal of Physics: Conference Series*, to be submitted before the end of November 2011.  
 [14] Dabrowski A. E. et al., Measuring the longitudinal bunch profile at CTF3, *Proceedings of LINAC10 conference* (2010).  
 [15] Brezinski C. and Redivo-Zaglia M., *Extrapolation methods theory and practice*, (ELSEVIER) (1991).